Journal of CO_2 Utilization 36 (2020) 288–294

Contents lists available at ScienceDirect

Journal of CO_2 Utilization

journal homepage: www.elsevier.com/locate/jcou

Transformation of the greenhouse gas carbon dioxide to graphene

Xinye Liu, Xirui Wang, Gad Licht, Stuart Licht*

Dept. of Chemistry, George Washington University, Washington DC 20052, USA

ARTICLE INFO

Keywords:
Graphene
Carbon dioxide electrolysis
Carbon nanoplatelets
Graphite exfoliation
Molten carbonate
Greenhouse gas mitigation

ABSTRACT

The deployment of graphene has been slow due to its high cost and high carbon footprint. A low carbon footprint, inexpensive synthesis of graphene, consuming rather than emitting CO_2, is introduced to overcome these obstacles. This is accomplished here by direct molten carbonate electrolytic splitting of the greenhouse gas CO_2 to a nano-thin carbon product (carbon nanoplatelets) comprised of 25–125 graphene layers, and subsequent electrochemical exfoliation of the nanoplatelets to graphene in a carbonate soluble aqueous solution. The sole products of the carbon dioxide electrolysis are straightforward: high yield carbon nanoplatelets and oxygen. The carbon nano platelets provides a thinner starting point than a conventional graphite reactant to facilitate electrochemical exfoliation. The resultant valuable product (graphene) incentivizes utilization of the greenhouse gas carbon dioxide.

Graphene has unique properties that are useful for a variety of applications. However, the synthetic costs and the challenge to isolate the graphene product in its native two dimensional structure lead to the high, current cost of graphene valued at approximately $1 million per ton [1]. Here, graphene is synthesized from CO_2 by (i) molten carbonate electrolysis to form carbon platelets on a stainless steel cathode. This is followed by cooling, and separation into individual graphene layers by (ii) high yield electrochemical exfoliation in a carbonate dissolving aqueous ammonium sulphate electrolyte. The electrosynthesized carbon platelets are nano-thin, promoting higher graphene yield than thicker, conventional graphite exfoliation reactions. CO_2 is the sole reactant used to produce the valuable product as graphene. This can incentivize utilization of CO_2, and unlike alternative products made from CO_2 such as carbon monoxide or other fuels such as methane [2,3], use of the product does release this greenhouse gas back into the atmosphere.

Graphene has a high surface area, high thermal and electrical conductivity, strength, surface tailorability, and high charge carrier conductivity that makes it uniquely suitable for energy storage and electronics [4–7]. It's ability to carry plasmons allows it to strongly interact with light in a non-linear fashion and both act as a transducer and transmitter in optoelectronics. Graphene's 2D honey-comb lattice sp^2 crystal structure possess extremely high intrinsic charge mobility (250,000 cm^2/Vs), a high specific surface area (2630 m^2/g), high thermal conductivity (5000 W/mK), high Young's modulus (1.0 TPa and high optical transmittance (97.7 %)). Methods to produce graphene include thermal annealing [8], unzipping nanotubes [9], solvothermal and thermal decomposition [10,11], ball-milling and chemical exfoliation [12,13], and CVD (chemical vapour deposition) [14–22]. CVD is a popular method to produce graphene from a variety of organometallics or other carbon sources and using transition metal catalysts. However, conventional CVD (chemical vapor deposition) can have a massive carbon footprint of over 600 tonnes of CO_2 per tonne of nanocarbon produced [23].

Another form of graphene synthesis is electrochemical exfoliation. As early as 2003 in an exploration of processes detrimental to Li-ion battery anodes, it was noted that electrochemical alkali ion intercalation could lead to peeling off of thin layers from graphite, and thin graphene-like exfoliated layers were clearly observed [24,25]. By 2007 the observation of one-atom thick graphene layers by electrochemical exfoliation was observed [26–28]. Electrochemical exfoliated graphene prepared from graphite is of increasing interest today, and is often mechanistically interpreted as an anodic process in which intercalated ions between the graphite layers are oxidized, forming gases which break the weak interlayer van de walls bounds, and release thin single or multi-layered graphene sheets into the electrolyte [29–32]. In 2017, it was observed that compression of graphite flakes prior to exfoliation, such as using graphite powder confined by wax coating could increase yield of graphene [33].

In the study here, we use confined carbon nano platelets, rather than graphite as a reactant to improve graphene yield. These ultra thin platelets are prepared directly and inexpensively from CO_2 as the sole reactant by electrolysis in molten carbonate electrolytes, providing a ready incentive to transform and utilize this greenhouse gas.

* Corresponding author.
E-mail address: slicht@gwu.edu (S. Licht).

https://doi.org/10.1016/j.jcou.2019.11.019
Received 15 August 2019; Received in revised form 3 November 2019; Accepted 12 November 2019

We recently discovered a high yield, high purity, (low) electricity cost constrained, carbon nanotube synthesis C2CNT (CO_2 to CNTs) [34–44]. The carbon platelet synthesis introduced in this study is an outgrowth of that discovery. Hence, C2CNT is briefly introduced here: C2CNT splits carbon dioxide by electrolysis in molten carbonates. Isotopic ^{13}C tracking was used to follow CO_2's consumption as it is dissolved in molten carbonate and is split by electrolysis to form the building blocks of CNTs [35]. CO_2 dissolution in molten lithium carbonate is exothermic and rapid, which along with heat generated by the electrolysis provides thermal balance during carbon deposition on the C2CNT cathode [43]. Transition metal nucleated electrolysis in lithium carbonate forms carbon nanotubes, oxygen and dissolved lithium oxide:

$$\text{Electrolysis: } Li_2CO_3 \rightarrow C_{CNT} + O_2 + Li_2O \quad (1a)$$

The Li_2CO_3 is effective either pure or with added oxides [34,35], added sodium, calcium, or barium carbonates [39,40], or added boron, sulfur, phosphorus or nitrogen dopants [40–42]. CO_2 added to the electrolyte dissolves and chemically reacts with lithium oxide to renew and reform Li_2CO_3:

$$\text{Chemical dissolution: } CO_2 + Li_2O \rightarrow Li_2CO_3 \quad (2)$$

Transition metals, such as Ni or Cr, nucleate CNT formation [34,38,40,41], and can be variously added to the electrolyte, added to the cathode or added by leach from the anode. The net reaction of Eqs 1 and 2 is CO_2 split by electrolysis to carbon nanotubes and oxygen:

$$CO_2 \rightarrow C_{CNT} + O_2 \quad (3)$$

In this study, rather than CNTs, carbon nanoplatelets are formed by molten carbonate electrolysis when other transition metals except zinc are excluded, and facilitated by increasing the electrolysis current in a step-wise manner prior to the constant current electrolysis:

$$\text{Electrolysis: } Li_2CO_3 \rightarrow C_{platelets} + O_2 + Li_2O \quad (1b)$$

The carbon platelets are converted to graphene by exfoliation:

$$\text{Exfoliation (DC voltage): } C_{platelets} \rightarrow C_{graphene} \quad (4)$$

As illustrated in Fig. 1, the net reaction of Eqs. 1b,2 and 4 is CO_2 split by electrolysis into graphene and oxygen:

$$CO_2 \rightarrow C_{graphene} + O_2 \quad (5)$$

Small transition metal clusters including Ni, Cr and others act as nucleation points to facilitate high yield C2CNT carbon nanotube growth [34–43]. Zinc, although liquid at molten carbonate temperatures lowered the energy of the initial carbon deposition [34,38]. In the absence of a solid transition metal as nucleating metal, galvanized (zinc coated steel) was still shown to be an effective cathode for carbon growth, but CNTs were scarce, comprising < 1 % of the carbon product. Instead the product, as shown in Fig. 2, is an impure mix of ultra-thin carbon platelets, other carbon nanostructures and amorphous carbon. Fig. 2 shows SEM of the washed cathode product from a nickel free, 90 min, 1 A constant current electrolysis in 730 °C molten Li_2CO_3 with 6 m (6 mol/kg Li_2CO_3) Li_2O (Alfa Aesar 99.5 %). The electrolysis uses a 5 cm^2 Pt foil anode and a 5 cm^2 0.12 cm diameter coiled galvanized steel wire cathode [34]. A mixture of nanostructures including a large fraction of platelets forms during the first few minutes of electrolysis, even in the presence of Ni. However, in the presence of Ni with extended electrolysis time the product quickly resolves into carbon nanotubes. This is the case with a wide range of lithiated electrolytes, using a wide range of metal cathodes including galvanized steel and copper, and over a range of electrolysis temperatures from 730 to 790 °C [34,39,49,41,42,43]. Higher temperatures, which are not used in this study, increasingly favor the two electron reduction of CO_2 to CO, and by 950 °C the product is pure carbon monoxide [2]. The formation of a transition metal nucleated carbon nanotube product is illustrated in Fig. 3. We use a copper cathode for this example, as we have specifically characterized by TEM the increase of CNT diameter and number of CNT wall layers for this cathode as a function of increasing electrolysis time.

Recently, we showed that in the absence of transition metal nucleating agents, carbon nano-onions (CNOs), rather than CNTs, form during molten carbonate electrolysis of CO_2 [44]. Here we show that in the absence of other transition metal nucleating agents, but in the presence of zinc, carbon nano platelets, rather than CNOs or CNTs form. Zinc is present as the surface coating on the (galvanized) steel cathode. The yield of carbon platelets observed in Fig. 2 increases to 70 % when the electrolyte is pure Li_2CO_3 rather than 6 m Li_2O, and to over 95 % when increasing constant current steps (Fig. 4B) are first applied prior to the constant current. Specifically, in this electrolysis, graphite platelets are grown on a 5 cm^2galvanized (zinc coated) steel cathode with a 5 cm^2 Pt Ir foil anode in 770 °C Li_2CO_3 when the electrolysis current is increased stepwise for 10 min. at 0.05 and 0.10 A, then 5 min. at 0.2 and 0.4 A followed by a constant of 1A for 2 h. These experimental conditions (zinc on the cathode, pure Li_2CO_3 electrolyte, neither Ni nor Cr in the anode, and increasing constant current steps) are chosen to increase the yield of the carbon platelets. Replicate experiments produced similar results of over 95 % carbon platelets yield. The 2 h constant current electrolysis occurs at 0.2 A cm^{-2}, consuming during the 2 h electrolysis 0.82 g CO_2 and producing 0.21 g carbon platelets. The potential of the stepped current electrolysis and the electrolysis product are presented in Fig. 4. The product purity is over 95 %. The remainder includes smaller particles, which also contain smaller platelets. XRD of the product in Fig. 4G exhibits a sharp peak at $2\theta = 26.3°$ indicative of a high degree of graphitic allotrope crystallinity. Raman spectroscopy Fig. 4F, and TEM 5A, indicates the platelets have a relatively low number (25–125) graphene layers. We hypothesize and will show that by starting with fewer graphene layers compared to graphite, these ultrathin platelets electrochemically exfoliate to a higher quality (thinner) graphene for an overall production of graphene from CO_2 by electrolysis and electrochemical exfoliation in accord with Eq. 5.

An important feature for the conversion of graphite to graphene is a red shift in the Raman spectrum 2D peak compared with graphite (2720 cm^{-1}) [45]. The 2D-band is highly sensitive to the number of graphene layers with single layer peak at 2679 cm^{-1}, and 1–4 layers at 2698 cm^{-1}. Even prior to electrochemical exfoliation the ultrathin carbon platelets produced by molten carbonate synthesis exhibit in Fig. 4F a significant red shift to 2708 cm^{-1}. In Fig. 4F the $I_D/I_{D'}$ is 1.3, demonstrating that for the whole range of $I_D/I_{D'}$ the defect level is always below the benchmark for graphene boundary defects ($I_D/I_{D'} = 3.5$) [45]. The ratio of Raman D or 2D to the G peaks are respectively associated with the number of defects and degree of graphitization [35]. In Fig. 4F, the intensity ratio of the Raman I_D/I_G peak is a low 0.4, and that of Raman $I_{2D}/I_G = 0.6$, which both indicate a small quantity of defects [46].

The net facile electrosynthesis of graphene from CO_2 is illustrated in Fig. 1 starting with the molten carbonate electrosynthesis of ultrathin graphite layers (1A), which provides a low carbon footprint and produces thinner graphene than a graphite foil exfoliation anode. Interestingly at the same constant exofoliation voltage, a similar current (0.79 $\pm$0.01 A) throughout the exfoliation, and a similar exfoliation time (10 h) is observed as was seen with a graphite reactant, as a graphite foil anode, using a similar configuration [46]. Here in lieu of graphite foil, the cooled extracted cathode containing both ultrathin graphite and congealed Li_2CO_3 electrolyte from the Fig. 4 molten carbonate synthesis is placed, without further treatment, in a closed cellulose tube immersed in 0.1 M aqueous ammonium sulfate (Alfa Aesar 99.5 %) as shown in Fig. 1B.

Unlike Na_2CO_3 and K_2CO_3 which are highly soluble in water, Li_2CO_3 has a low solubility (30.6, 113 and 1.2 g per 100 g H_2O respectively at 25 °C). We have previously shown that aqueous ammonium sulfate is one of the few media in which Li_2CO_3 solubility is enhanced [41], and its solubility is delineated in the supplementary data.

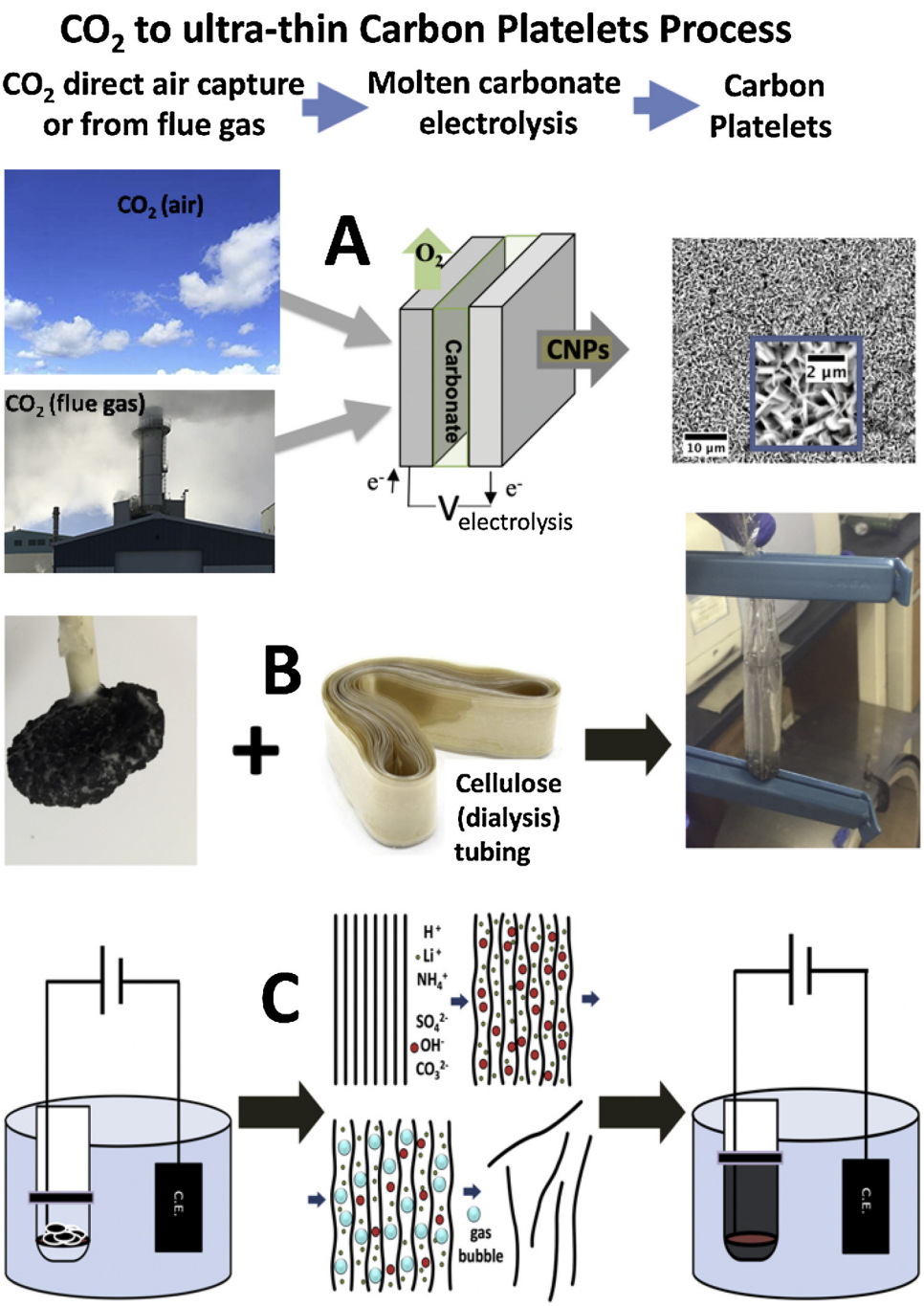

Fig. 1. Electrosynthesis of graphene from CO_2. A: CO_2 from the air or from flue gas is electrolytically split to ultra-thin graphene platelets product by molten carbonate electrolysis. B: The carbonate synthesis cathode containing product is cooled and placed in a cellulose tube containing aqueous $(NH_4)_2SO_4$. C: The cellulose tube is placed in an $(NH_4)_2SO_4$ bath with a counter electrode; DC voltage is applied that generates gas bursts between the graphene layers exfoliating the thin platelets producing graphene.

Securing the electrochemical exfoliation electrode within a cellulose dialysis membrane can isolate the graphene product from the bulk electrolyte [47]. The electrode within a cellulose membrane assembly is used as the anode in a two-compartment electrochemical cell, but rather than using graphite, using the cooled cathode, unwashed (carbon nanoplatelet) cathode in 0.1 M $(NH_4)_2SO_4$ as shown in Fig. 1C. Specifically, the carbonate synthesis cathode containing product is cooled and placed in a cellulose tube containing aqueous 0.1 M $(NH_4)_2SO_4$. The cellulose tube is an inexpensive premium commercial cellulose dialysis membrane, (https://www.amazon.com/s?k = Premium-Dialysis-Tubing-Regenerated-Cellulose) listed as a cutoff of 12–14 kdals, equivalent to 1–2 nm pore size. As shown in Fig. 1C, the cellulose tube is placed in an 0.1 M $(NH_4)_2SO_4$ bath with a counter electrode; 10 V DC voltage is applied that generates gas bursts between the graphene layers exfoliating the thin platelets producing graphene. As graphene layers are peeled, the cellulose traps them within the anode compartment.

Before exfoliation the platelets range from 25–125 graphene layers as measured by TEM (representative example Fig. 5A), and consistent with the measured Raman spectrum 2D peak (graphite red shifted) at 2708 cm^{-1}. After exfoliation, the lateral dimensions of the exfoliated layers are 3–8 µm as measured by SEM (Fig. 5B), which has been slightly colorized to enhance contrast.

After exfoliation the product is filtered, rinsed and freeze dried to remove water, and studied by TEM, AFM and Raman. The exfoliation

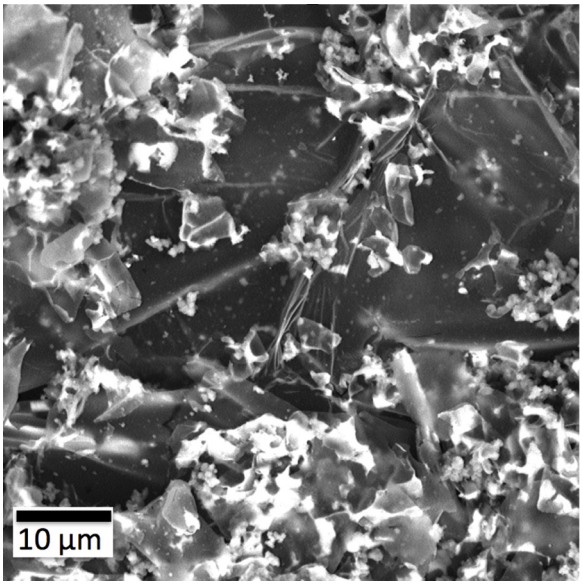

Fig. 2. In the absence of nickel nucleation and in the presence of zinc, molten carbonate electrolytic splitting of CO_2 forms carbon platelets. SEM of the product exhibits a mix of platelets and amorphous carbon. Ni-free electrolysis is conducted for 90 min at 1 A constant in 730 °C molten Li_2CO_3 with 6 m Li_2O using conducted using a 5 cm^2 Pt foil anode and a 5 $cm^2$0.12 cm diameter coiled galvanized steel wire cathode. SEM is measured with a PHENOM Pro-X SEM.

product yield is 83 % by mass of the original carbon platelets and presumably yield would rise with longer (than 10 h) exfoliation time.

In Fig. 5C, the Raman 2D peak exhibits a significant red shift from 2708 to 2690 cm^{-1} from platelets (pre-exfoliation) to graphene (post-exfoliation), product and each are red shifted from graphite (2720 cm^{-1}). This shift to 2690 cm^{-1} is indicative of graphene ranging from to 1–5 graphene layers thick. Edge TEM cross section of the exfoliation product also exhibits graphene ranging from 1 layer (shown in the Fig. 5B inset) to 5 layers thick. This is verified by AFM (Fig. 5D). Dispersion of the graphene product for AFM characterization remains a challenge; sonication and freeze drying effectively disperses, but is overly aggressive and converts the graphene from a continuous flake to "swiss cheese," which has the benefit of providing extra locations for depth determination (Fig. 5D). For comparison, graphite foil as the exfoliating reactant, rather than the molten carbonate synthesized carbon nanoplatelets in the same experimental configuration, produces multilayered graphene that is approximately 5 fold thicker, and ranges from 6 to 25 graphene layers thick (and the 2D-band peak at ~2703 cm^{-1}, rather than 2690 cm^{-1} observed for the carbon nanoplatelet exfoliated product.

Raman of the graphene indicates that the exfoliation product exhibits increased defects compared to thicker pre-exfoliation platelets formed during electrolysis in molten carbonate, but the defect level remains low and within tolerated levels for graphene. From Fig. 5C peak ratios for graphene are compared to ratios for the platelets: the $I_D/I_{D'}$ is 1.5 (1.3), again demonstrating that for the whole range of $I_{D/}I_{D'}$ the defect level is always below the benchmark for graphene boundary defects of $I_D/I_{D'}$ = 3.5 [45]. The intensity ratio of the Raman I_D/I_G peak is 0.64 (0.4), and that of Raman I_{2D}/I_G is 0.70 (0.6), which both indicate a small quantity of defects.

In addition to carbon nanoplatelets the second product of molten carbonate CO_2 electrolysis in Eq. 5 is O_2, and the evolution of pure oxygen during the electrolysis has been demonstrated [43]. We suggest that with completion of this proof of concept stage, several of the synthesis parameters can be substantially optimized. For example, the majority of the applied exfoliation 10 V is lost through resistance drop over the 0.1 M ammonium sulfate solution and this can be avoided by closer electrodes and higher ionic strength to lower energy requirements. The temperature can be increased and the cellulose membrane can also be modified to minimize the voltage drop and also increase the sustainable current density (and rate of exfoliation). The noble iridium/platinum anode is purposely used here to inhibit CNT formation. This enhances the observed formation of the desired graphene product by preventing introduction from the anode, migration, reduction and formation of nickel or chromium nucleation sites on the cathode that could have favored formation of the alternative CNT product as we have demonstrated in other studies [34–43]. However, an Ir, Pt or Ir alloy anode is not a prerequisite for high yield graphene growth. The inhibition of low levels of Ni migration from a Ni or Ni containing alloy anode or use of a thin film Ir anode are planned. In the supplementary data, we reference some of the many relevant studies on thin film iridium deposition.

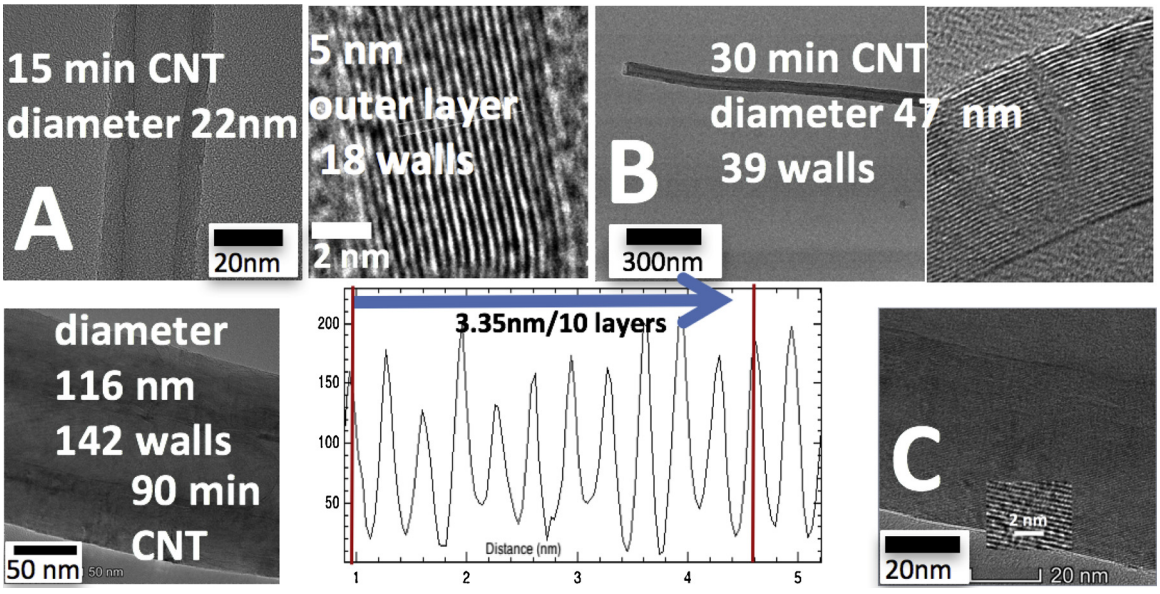

Fig. 3. With nucleation, molten carbonate electrolytic splitting of CO_2 forms carbon nanotubes. TEM of the electrolysis product subsequent to A: 15, B: 30 or C: 90 min of 1 A electrolysis in 770 °C Li_2CO_3 at a 5 cm^2 copper with Ni powder; the anode is a 5 cm^2Pt Ir foil. CNT diameter and number of wall layers increases in time. TEM are measured by FEI Teneo Talos F200XTEM.

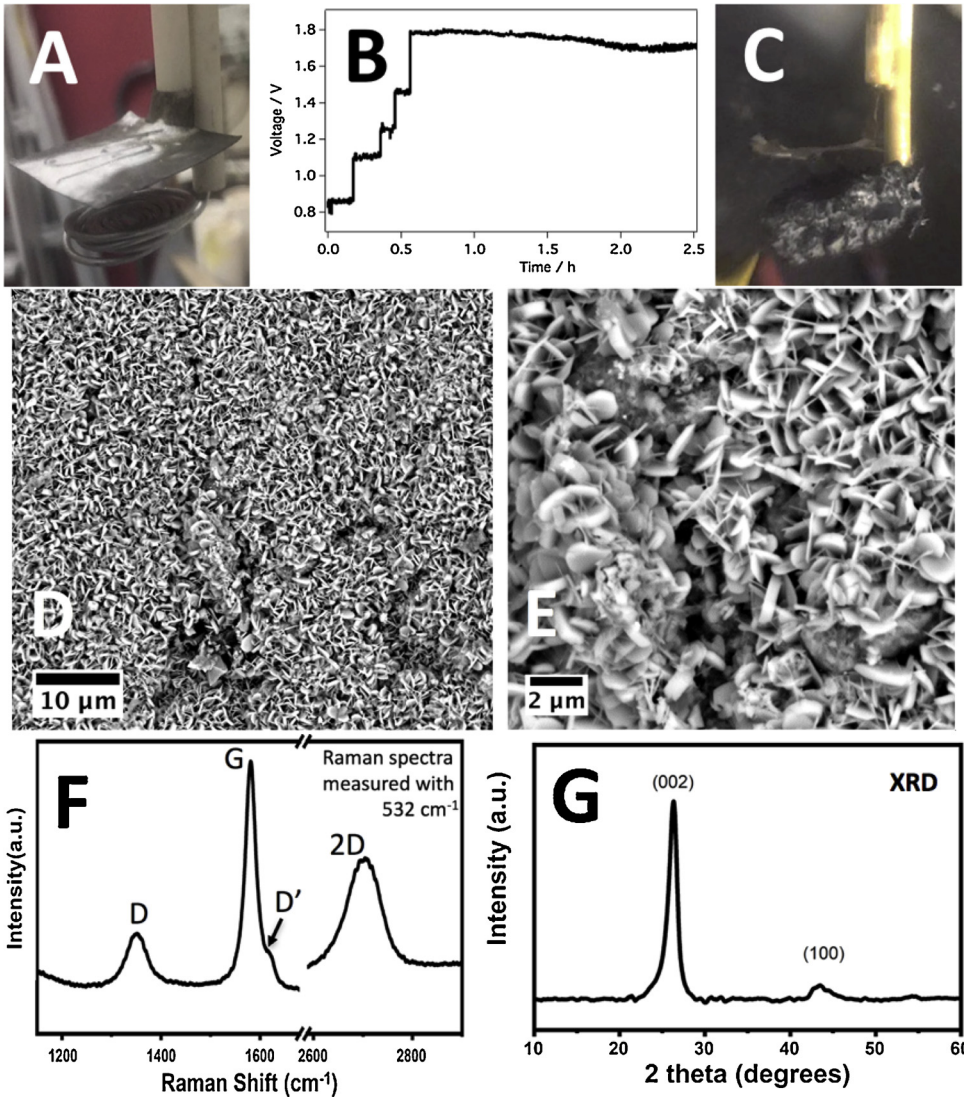

Fig. 4. Electrosynthesis of carbon platelets from CO_2. A: CO_2 Pure (over 95 %) ultrathin graphite platelets are grown on a 5 cm^2galvanized (zinc coated) steel cathode with a 5 cm^2 Pt Ir foil anode in 770 °C Li_2CO_3 when the electrolysis current is increased stepwise for 10 min. at 0.05 and 0.10 A, then 5 min. at 0.2 and 0.4 A followed by a constant of 1A for 2 h. Panels A & C are the electrodes before and then after electrolysis. B: Measured cell potential during the electrolysis. D & E: SEM of the washed cathode product at low and high magnification. F & G: Raman and XRD spectra of the product. Raman spectroscopy was measured with a LabRAM HR800 Raman microscope (HORIBA) using 532.14 nm wavelength incident laser light with a resolution of 0.6 cm^{-1}, and XRD with a Rigaku D = Max 2200 XRD.

Except for the noble-metal anode, all components of the molten carbonate electrolytic transformation of CO_2 to graphene are inexpensive. The transformation bears many similarities to the production of aluminum, and may be compared to the established costs of this latter, mature industry. In the 19th century aluminum was more expensive than gold with little market. However, via a change of chemical technology today aluminum is inexpensive with a mass market. Both processes entail the straightforward, high current density, molten electrolytic electrochemical reduction of an oxide, and do not use noble or exotic materials. CO_2 electrolysis in molten carbonate production of carbon nanomaterials readily scales upward linearly with the area of the electrolysis electrodes [34,43], facilitating the analogous larger scale synthesis of graphene. The aluminum electrolysis uses and consumes a carbon anode that emits carbon dioxide, whereas the molten carbonate carbon nanomaterial electrolysis anode is not consumed and emits oxygen. 52 % ($977) of the $1880 per tonne cost of Al production consists of bauxite and carbon [48]; whereas this molten carbonate electrolysis does not consume carbon as a reactant and uses a no-cost oxide as the reactant to be reduced (CO_2, rather than mined bauxite). As detailed in our recent carbon nanotube syntheses, molten carbonate CO_2 electrolyses costs are similar, but less expensive than the industrial production of aluminum [41,42].

In addition to a higher carbon footprint, the aluminum process necessitates a larger physical footprint. Aluminum production uses the higher density of liquid aluminum compared to the density of the fluoride electrolyte to collect the aluminum product from a horizontal electrode; whereas the nanocarbon product resides on the cathode, which therefore may be stacked vertically in a low physical footprint configuration. The carbon nanomaterial molten carbonate electrolysis process operates under somewhat milder conditions at 770 °C in a less exotic, molten carbonate electrolyte at similar rates of output, but at a lower 0.7–2 V [37] potential compared to an electrolysis potential of over 4 V for aluminum, and the electricity costs per tonne are estimated as $360 compared to the known costs of $602 per tonne for aluminum. As a first order estimate of the per tonne similarity with the known capital ($150, consisting primarily of electrolysis kilns in series, and current rectifiers) and labor costs ($150) with the aluminum process. More accurate first-hand knowledge of both CAPEX and labor of molten carbonate splitting of CO_2 are being conducted at the C2CNT scale-up in the ongoing Carbon XPrize as delineated at CarbonXPrize.com and C2CNT.com.

Hence, $1000 is a reasonable upper bound estimation to industrial carbon graphene production by carbon dioxide electrolysis, excluding anode and exfoliation costs to be determined, in molten carbonates. This cost is significantly lower than the current price of graphene, and may provide a significant incentive to use the greenhouse gas carbon dioxide as a reactant to produce carbon graphene. This can provide a useful path forward to help break the anthropogenic carbon cycle to

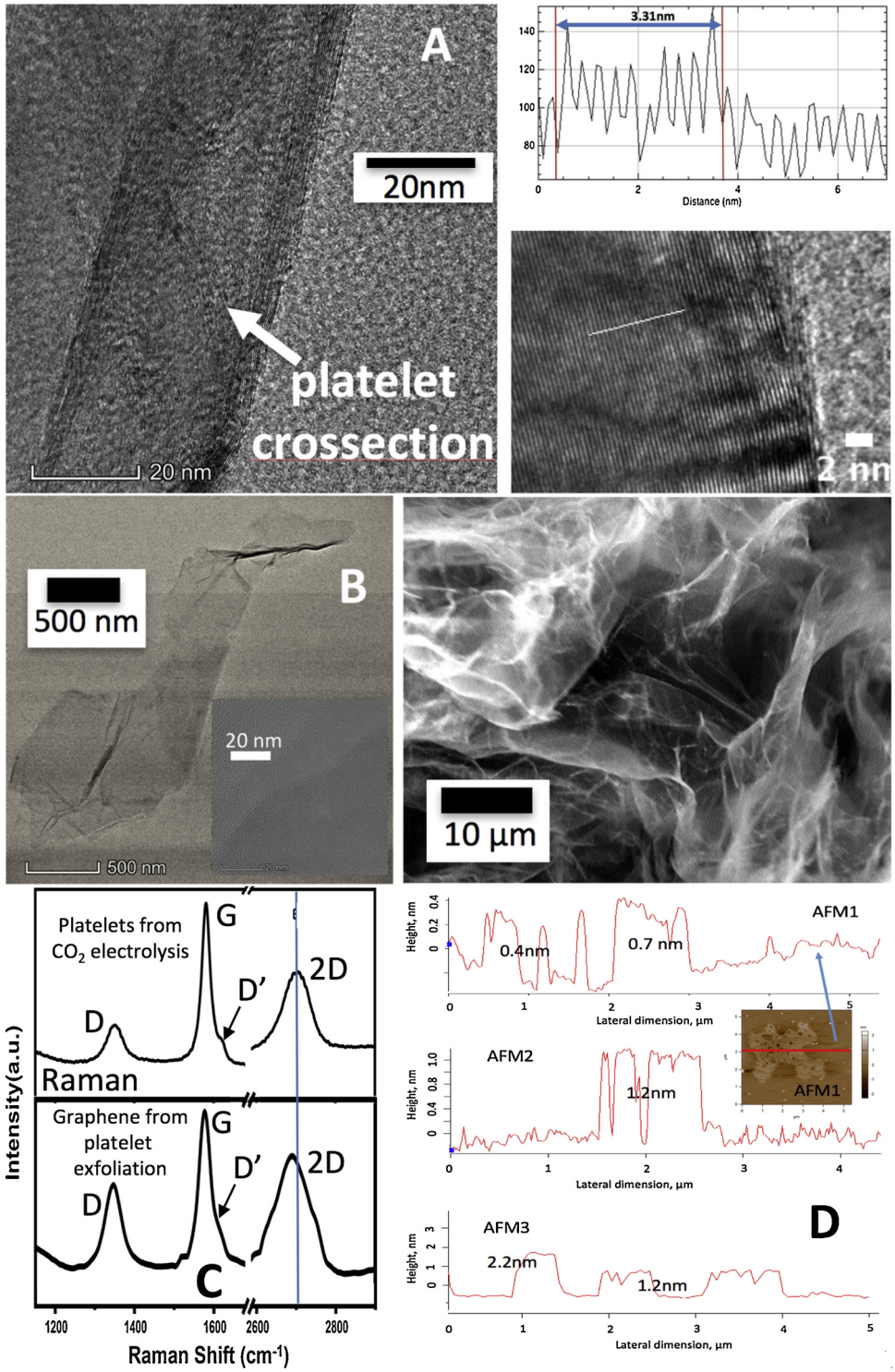

Fig. 5. Electrosynthesis of graphene from CO_2. Carbon platelets contain a range of 25–125 graphene layers prior to exfoliation and range from 1–5 graphene layers following exfoliation. A: Representative SEM of the platelets prior to exfoliation as the product of CO_2 electrolysis in molten carbonate. B: Subsequent to exfoliation representative SEM of the graphene product. B inset: Edge TEM cross section of 1 carbon layer thick exfoliation product. C: Raman and D: AFM of the graphene product. Atomic force microscopy was tapping mode imaged with an Asylum MFP-3D AFM.

mitigate climate change.

1. Conclusions

A novel facile electrosynthesis of graphene from CO_2 has been presented, which overcomes the challenges of high cost and high carbon footprint that had hampered deployment of applications that take advantage of the unique, advantageous physical chemical properties of graphene. This is accomplished by molten carbon synthesis of nano-thin carbon platelets, and subsequent electrochemical exfoliation of the platelets into graphene. The graphene produced has a thickness of 1–5 carbon layers, but a relatively small lateral dimension of 2–8 µm. This lateral size is for example of use in graphene as a lubricant, in battery anodes, and in graphene admixture applications. Larger lateral

dimensions would expand the utility of the molten carbonate electrolysis. This study is intended as a proof of concept demonstration. Future variations of the condition, for example variation of the molten carbonate synthesis electrolysis time and use of a binary or ternary carbonate mixture to lower viscosity have a high probability to increase the graphene lateral dimension. Furthermore, to introduce the new synthesis in a logical stepwise manner, although the carbon nanoplatelet component of the synthesis is unconventional, conventional exfoliation conditions were utilized with the principle differences being the use of (i) ultrathin molten carbonate carbon platelets to facilitate graphene exfoliation and (ii) using carbon sourced from CO_2 electrolysis, rather than using commercial graphite as the exfoliation anode to decrease the carbon footprint of graphene production. As discussed in the study, it is likely that in future variations of this new synthesis the requisite exfoliation voltage can be substantially decreased.

Here, graphene is synthesized to high yield from the greenhouse gas CO_2 by (i) electrolysis in a molten carbonate to form carbon platelets at high yield on a galvanized steel cathode, followed by cooling and placing the cathode within a cellulose membrane and (ii) then high yield exfoliation of the platelets as an anode in a carbonate dissolving aqueous ammonium sulfate solution and generating gas between the graphene layers to promote separation of the individual graphene layers. The produced molten carbonate synthesized platelets are nano-thin and promote fewer carbon layers in the product and higher yield than thicker, conventional graphite exfoliation reactions. Utilization of CO_2 as the sole reactant produces graphene as a low carbon footprint product.

Declaration of Competing Interest

The authors declare that there are no conflicts of interest.

Acknowledgements

We are grateful to Michael Keidar for use of the Raman instrumentation, to Santiago Solares and Berkin Uluutku for use of the AFM instrumentation, and to C2CNT for support of this research

Appendix A. Supplementary data

Supplementary data associated with this article can be found, in the online version, at https://doi.org/10.1016/j.jcou.2019.11.019.

References

[1] Price and Market of Materials, Carbon XPrize Standards Data Summary Set, Draft V1.2, (2017) Sept. 12.
[2] S. Licht, B. Wang, S. Ghosh, H. Ayub, D. Jiang, J. Ginley, J. Phys. Chem. Lett. 1 (2010) 2363–2368.
[3] H. Wu, D. Ji, L. Li, D. Yuan, Y. Zhu, B. Wang, Z. Zhang, S. Licht, Adv. Mater. Technol. 5 (2016) 1600092 1.
[4] M. Coroş, F. Pogaceăn, L. Măgeruşsan, C. Socaci, S. Pruneanu, Front. Mater. Sci. 13 (2019) 23.
[5] E.S. Agudosi, E.C. Abdullah, A. Numan, N.M. Mubarak, M. Khalid, N. Omar, Crit. Rev. Mater. Sci. 1040-8436 (2019) 1.
[6] X.L. Bai, Y. Zhang, W. Tong, L. Sun, H. Huang, Q. An, N. Tian, P.K. Chu, Electrochem. Energy Rev. (2019), https://doi.org/10.1007/s41918-019-00042-6.
[7] Z. Zhang, X. Xu, L. Qiu, S. Wang, T. Wu, F. Ding, H. Peng, K. Lu, Adv. Sci. 1700087 (2017) 4.
[8] C. Li, D. Li, J. Yang, X. Zeng, W. Yuan, J. Nanomater. 2011 (2011) 319624.
[9] H. Tanaka, R. Arima, M. Fukumori, D. Tanaka, R. Negishi, Y. Kobyayashi, S. Kasai, T.K. Yamada, T. Ogawa, Sci. Rep. 5 (2015) 12341.
[10] D.K. Singh, P.K. Iyer, P.K. Giri, Int. J. Nanosci. 10 (2019) 39.
[11] C. Berger, Z. Song, T. Li, X. Li, A.Y. Ogbazghi, R. Feng, Z. Dai, A.N. Marchenkov, E.H. Conrad, P.N. First, W.A. de Heer, J. Phys. Chem. B 108 (2004) 19912.
[12] A.E. Del Tio-Castillo, C. Merino, E. Diez-Barra, E. Vazques, Nano Res. 7 (2014) 963.
[13] M. Liu, X. Zhang, W. Wu, T. Liu, Y. Liu, B. Guo, R. Zhang, Chem. Eng. J. 355 (2019) 181.
[14] S. Shukla, S.-Y. Kang, S. Saxena, Appl. Phys. Rev. 6 (2019) 021331.
[15] M.A. Azam, N.N. Zulkpli, N. Dorah, R.N.A.E. Seman, M.H. Ani, M.S. Sirat, E. Ishail, F.B. Fauzhi, M.A. Mohamed, B.Y. Majlis, ECS J. Solid State Sci. Technol. 6 (6) (2017) M3035.
[16] H.C. Lee, W. Liu, S. Chai, A.R. Mohamed, A. Aziz, C. Khe, N.M.S. Hidayaha, U. Hashima, RSC Adv. 7 (2017) 15644.
[17] Z. Zhang, X. Xu, L. Qiu, S. Wang, T. Wu, F. Ding, H. Peng, K. Lu, Adv. Sci. 1700087 (2017) 4.
[18] H. Sun, J. Xu, C. Wang, G. Ge, Y. Jia, J. Liu, F. Song, J. Wan, Carbon 108 (2016) 356.
[19] Z. Yan, Z. Peng, J.M. Tour, Acc. Chem. Res. 47 (2014) 1327.
[20] C.-M. Seah, S.C. Chai, A.R. Mohamed, Carbon 70 (2014) 1.
[21] D.Y. Lee, C.Y. Shin, S.J. Yoon, H.Y. Lee, W. Lee, N.K. Shrestha, J.K. Lee, S.-H. Han, Sci. Rep. 4 (2014) 3930.
[22] S. Das, M. Kim, J. Lee, E. Choi, Crt. Rev. Sol. State Mater. Sci. 39 (2014) 231.
[23] V. Khanna, B.R. Bakshi, L.J. Lee, J. Ind. Ecol. 12 (2008) 394.
[24] H. Buqa, D. Goers, L. Hardwick, M.E. Spahr, P. Novak, US DOE Tech. Rep. ETDE-CH-0301 (2003) 63.
[25] M.E. Spahr, T. Palladino, H. Wilhelm, A. Wursig, D. Goers, H. Buqa, M. Holzapfel, P. Novak, J. Electrochem. Soc. 151 (2004) 181.
[26] A. Penicaud, L. Valat, A. Derre, P. Poulin, C. Zakri, O. Roubeau, M. Maugey, P. Miaudet, E. Anglaret, P. Petit, A. Loiseau, S. Enouz, Compos. Sci. Technol. 67 (2007) 795.
[27] A. Mansour, M. Razafinimanana, M. Monthioux, M. Pacheco, A. Gleizes, Carbon 45 (2007) 1651.
[28] C. Valles, C. Drummond, H. Saadaoui, C.A. Furtado, M. He, O. Roubeay, L. Ortlani, M. Monthioux, A. Penicaud, J. Am. Chem. Soc. 130 (2008) 15802.
[29] H. Hashimoto, Y. Muramatsu, Y. Nishina, H. Asoh, Electrochem. Comm. 104 (2019) 106475.
[30] Z. Xia, M. Christian, C. Arbizzani, V. Morandi, M. Gassano, V. Quintano, A. Kovtun, V. Palermon, Nanoscale 11 (2019) 5265.
[31] E.S. Bakunin, E.Y. Obraztsova, A.V. Rukhov, Inorg. Mat.: Appl Res. 10 (2019) 249.
[32] I. Khahpour, A. Baboukani, A. Allagui, C. Wang, Appl. Energy Mat. 2 (2019) 4813.
[33] H. Wang, C. Wei, K. Zhu, Y. Zhang, C. Gong, J. Guo, J. Zhang, L. Yu, J. Zhang, Appl. Mat Interfaces 9 (2017) 34456.
[34] J. Ren, F. Li, J. Lau, L. Ganzalez-Urbina, S. Licht, Nano Lett. 15 (2015) 6142.
[35] J. Ren, S. Licht, Sci. Rep. 6 (2016) 27760.
[36] S. Licht, A. Douglas, R. Carter, M. Lefler, C. Pint, ACS Cent. Sci. 2 (2015) 162.
[37] J. Ren, J. Lau, M. Lefler, S. Licht, J. Phys. Chem. C 119 (2015) 23342.
[38] G. Dey, J. Ren, T. El-Ghazawhi, S. Licht, RSC Adv. 6 (2016) 27191.
[39] H. Wu, Z. Li, D. Ji, Y. Liu, L. Li, D. Yuan, Z. Zhang, J. Ren, M. Lefler, B. Wang, S. Licht, Carbon 106 (2016) 208.
[40] J. Ren, M. Johnson, R. Singhl, S. Licht, J. CO_2 Util. 18 (2017) 335.
[41] M. Johnson, J. Ren, M. Lefler, G. Licht, J. Vicini, X. Liu, S. Licht, Mater. Today Energy 5 (2017) 230.
[42] M. Johnson, J. Ren, M. Lefler, G. Licht, J. Vicini, X. Liu, S. Licht, Data Brief 14 (2017) 592.
[43] X. Wang, X. Liu, G. Licht, B. Wang, S. Licht, J. CO_2 Util. 34 (2019) 303.
[44] X. Liu, J. Ren, G. Licht, X. Wang, S. Licht, Adv. Sust. Mater. 1900056 (2019) 1.
[45] Q. Zhou, Y. Lu, H. Xu, Mater. Lett. 235 (2019) 153.
[46] T.C. Achee, W. Sun, J.T. Hope, S.G. Quitzau, C.B. Sweeny, S.A. Shah, T. Habib, M.J. Green, Sci. Rep. 8 (2018) 14525.
[47] N. K. Chaki, et al., US Pat. Appl., 2018, Pub No.: US2018/0072573.
[48] G. Djukanovic, Int. Aluminium J. 7-8 (2012) 28–32.